



## Article

# Reduced-Dynamic Precise Orbit Determination of Haiyang-2B Altimetry Satellite Using a Refined Empirical Acceleration Model

Youcun Wang <sup>1</sup>, Min Li <sup>1,\*</sup>, Kecai Jiang <sup>1</sup>, Wenwen Li <sup>1</sup>, Geer Qin <sup>1</sup>, Qile Zhao <sup>1</sup>, Hailong Peng <sup>2</sup> and Mingsen Lin <sup>2</sup>

<sup>1</sup> GNSS Research Center, Wuhan University, Wuhan 430079, China; youcunwang@whu.edu.cn (Y.W.); kc.jiang@whu.edu.cn (K.J.); cheeselee@whu.edu.cn (W.L.); 2014301610210@whu.edu.cn (G.Q.); zhaoql@whu.edu.cn (Q.Z.)

<sup>2</sup> National Satellite Ocean Application Service, Beijing 100081, China; phl@mail.nsoas.org.cn (H.P.); mslin@mail.nsoas.org.cn (M.L.)

\* Correspondence: limin@whu.edu.cn; Tel.: +86-027-6877-8767

**Abstract:** The Haiyang 2B (HY-2B) satellite requires precise orbit determination (POD) products for geodetic remote sensing techniques. An improved set of reduced-dynamic (RD) orbit solutions was generated from the onboard Global Positioning System (GPS) measurements over a 14-month period using refined strategies and processing techniques. The key POD strategies include a refined empirical acceleration model, in-flight calibration of the GPS antenna, and the resolution of single-receiver carrier-phase ambiguities. In this study, the potential periodicity of empirical acceleration in the HY-2B POD was identified by spectral analysis. In the along-track direction, a noticeable signal with four cycles per revolution (CPR) was significant. A mixed spectrum was observed for the cross-track direction. To better understand the real in-flight environment, a refined empirical acceleration model was used to cope with the time variability of empirical accelerations in HY-2B POD. Three POD strategies were used for the reprocessing for superior orbit quality. Validation using over one year of satellite laser ranging (SLR) measurements demonstrated a 5.2% improvement in the orbit solution of the refined model. Reliable correction for the GPS antenna phase center was obtained from an over-420-day dataset, and a trend in radial offset change was observed. After application of the in-flight calibration of the GPS antenna, a 26% reduction in the RMS SLR residuals was achieved for the RD orbit solution, and the carrier phase residuals were clearly reduced. The integer ambiguity resolution of HY-2B led to strong geometric constraints for the estimated parameters, and a 15% improvement in the SLR residuals could be inferred compared with the float solution.



**Citation:** Wang, Y.; Li, M.; Jiang, K.; Li, W.; Qin, G.; Zhao, Q.; Peng, H.; Lin, M. Reduced-Dynamic Precise Orbit Determination of Haiyang-2B Altimetry Satellite Using a Refined Empirical Acceleration Model. *Remote Sens.* **2021**, *13*, 3702. <https://doi.org/10.3390/rs13183702>

Academic Editor: Ali Khenchaf

Received: 17 August 2021

Accepted: 13 September 2021

Published: 16 September 2021

**Publisher's Note:** MDPI stays neutral with regard to jurisdictional claims in published maps and institutional affiliations.



**Copyright:** © 2021 by the authors. Licensee MDPI, Basel, Switzerland. This article is an open access article distributed under the terms and conditions of the Creative Commons Attribution (CC BY) license (<https://creativecommons.org/licenses/by/4.0/>).

**Keywords:** HY-2B; precise orbit determination; empirical accelerations model; satellite laser ranging; GPS antenna phase center; single-receiver ambiguity resolution

## 1. Introduction

HaiYang-2B (HY-2B) is the second marine dynamic environment satellite of China [1]. It was launched on 25 October 2018, with an altitude and inclination of about 973 km and 99.3°, respectively. The major objective of the HY-2B is to monitor and investigate the marine environment. It carries various instruments, including a dual-frequency altimeter in the Ku and C-bands, a scatterometer, and a microwave imager. The HY-2B mission undertakes routine measurements of sea surface height. Its precise orbit provides a good reference for an altimetry satellite, which is very important for long-term Earth observation missions [2–4]. Moreover, the precise orbit determination (POD) function of the altimetry satellite is the basis of various oceanographic applications based on altimetry technology [5,6], such as the determination of global and regional mean sea level changes, the modeling of the mean sea height, ocean tide simulations, etc. [7–9].

To support this mission, the HY-2B spacecraft hosts a POD package, including an onboard Global Positioning System (GPS) receiver and a laser retroreflector (LRR) for

satellite laser ranging (SLR). Based on Global Navigation Satellite System (GNSS) measurements and dynamical models of satellites, three different orbit determination methods were developed, which are known as kinematic, dynamic, and reduced-dynamic. To optimize the advantages of purely geometric observations and dynamic methods, pseudo-stochastic parameters are employed to compensate for potential deficiencies of dynamic models based on reduced-dynamic concepts [5,10]. At present, the reduced-dynamic POD based on onboard GNSS observations has been widely used for most low-Earth orbit (LEO) geodetic [11–13] and remote sensing missions [14–16]. The precise orbits of GRACE [17], with an uncertainty of less than 3 cm in SLR residuals, are supported using onboard GPS data. Overall SLR validation better than 2 cm for GOCE missions can be obtained for GPS-based orbits [18]. The reduced-dynamic Swarm Precise Science Orbits (PSO) showed an accuracy of better than 2 cm by independent SLR validation [19,20]. However, the dynamic background models of the satellites involved and their data processing strategies differ slightly, and there is no unified POD strategy.

Empirical accelerations have been successfully used in LEO POD as an inherent strategy. Along with the initial state vector of LEO satellites and the scaling factors for individual force model constituents, empirical acceleration parameters are estimated in reduced-dynamic POD. The performance of this technique in high-precision orbit determination has been widely investigated by the LEO POD community [21–23]. A refined non-gravitational force model of a LEO satellite will reduce the amount of empirical acceleration [13,23,24], and many scholars have set their sights on model refinement. Some analysis has indicated the direction and the time variability of the remaining deficit [18,22]. From the perspective of spectral analysis, the potential perturbation frequency of unmodeled acceleration information can be extracted and analyzed. Better orbit determination results may be obtained when the empirical acceleration is consistent with the spectral analysis. Therefore, spectral analysis of the remaining empirical acceleration of POD was performed, and an optimized piece-wise empirical acceleration (PEA) model is proposed in this article.

The accurate known location of the GPS receiver antenna relative to the center of mass (CoM) is the premise of precise orbit determination [25,26]. This location is typically provided by the spacecraft manufacturer, with a nominal accuracy of millimeters or better, but the experience of past geodetic missions has shown that there may be inconsistencies at the level of 2–3 cm [16,27,28]. Therefore, offset calibration of the GPS antenna phase center and empirical phase center variations (PCV) corrections were performed to eliminate the systematic errors in the HY-2B POD. Single-receiver integer ambiguity resolution (IAR) has often been implemented in numerous LEO missions, and improved precision can be inferred from SLR validation [13,16,20]. Unlike the fixed double-difference ambiguity of terrestrial stations, a single-receiver IAR depends on the dedicated GNSS orbit, clocks, and wide-lane bias products [16,29,30], which were implemented in this study to improve orbit solutions. The single-receiver IAR of the Sentinel-3 and Swarm missions based on the GRG (Groupe de Recherche de Géodésie Spatiale) products of the CNES/CLS (Centre National d'Études Spatiales/Collecte Localisation Satellites) [31] analysis center is supported by previous studies [16,20]. Furthermore, GNSS orbits and an IAR-enabled clock with the accompanying Observation-Specific Bias (OSB) provided by the Center for Orbit Determination in Europe (CODE) [30] was used to implement the single-receiver IAR of LEO missions [13]. For improved orbit solutions for the HY-2B, a single-receiver IAR was implemented in this study.

This manuscript is organized as follows. Section 2 provides a brief introduction to the background dynamic model and the data process strategy used in HY-2B POD. An assessment and a discussion of the different orbit solutions are presented in Section 3. A discussion about the results is provided in in Section 4. Finally, Section 5 concludes the study and provides a general outlook.

## 2. Spectral Analysis of HY-2B Empirical Accelerations

The process models and strategies used for the determination of the HY-2B orbit are elaborated in this section. The GNSS Research Center of Wuhan University undertakes routine POD for the associated Haiyang-2 satellites, and the preliminary motivation of this work was to improve the accuracy of the HY-2B satellite POD. The improvements were driven primarily by offset calibration of the GPS antenna, implementation of ambiguity resolution, and a refined PEA model.

### 2.1. POD Processing and Models

The reduced dynamic POD method makes use of GPS observations and well-established models for computing the acceleration acting on satellites. An overview of the supporting models and data processing strategies is presented in Table 1. The undifferenced processing was adopted, and dual-frequency ionosphere-free combinations of the GPS data were used as the basic observations for the HY-2B POD. The precise GNSS orbits, clock, and wide-lane bias products provided by the CNES/CLS were used to implement a single-receiver IAR for the HY-2B satellite. In order to be consistent with the standard IGS clock product, GPS observations with a measurement interval of 30 seconds were used. For processing GPS data with a sampling interval of below 30 seconds, the high-rate GRG clock offsets based on the CODE clock product is available for single-receiver IAR. Details of this concept and its implementation are described [20]. The GPS transmitter antenna phase center offsets (PCO) and PCV of the IGS model [32,33] were taken into account. The GPS antenna offset calibration of the HY-2B and the empirical PCV corrections were considered in POD.

**Table 1.** Force models and datasets for HY-2B precise orbit determination and SLR validation.

Model	Description
<b>Observation model</b>	
Observation	Undifferenced ionosphere-free code and carrier phase combinations
Interval and arc length	30 s and 30 h
GPS orbit and clocks	CNES-CLS ‘GRG’ products; 30 s sampling
GPS satellite biases	CNES-CLS wide-lane satellite biases
GPS satellite PCO and PCV	IGS ATX models [33]
HY-2B attitude	Nominal
HY-2B PCO and PCV	Corrected using calibrated values
<b>Dynamic model</b>	
Earth gravity	EIGEN6C (120 × 120) [34]
Solid Earth and pole tides	IERS 2010 conventions [35]
Ocean tides	FES 2004 (30 × 30) [36]
N-body disturbance	JPL DE405 [37]
Relativity	IERS 2003 [38]
Solar radiation	13-plate macro-model, radiation pressure coefficients (VIS and IR) [39]
Atmospheric drag	13-plate macro-model, atmospheric density model adopting DTM-2013 [40]
Empirical acceleration	Piecewise periodic acceleration
<b>Estimated parameters</b>	
Initial state	Position and velocity at the initial epoch
Receiver clock offset	Each epoch as white noise
Phase ambiguities	Each continuous tracking arc as a float
Solar radiation coefficients	One per 30 h arc
Drag coefficients	One per 180 min
Empirical coefficients	One per 180 min, amplitudes of periodic accelerations acting on the along- and cross-track directions

Table 1. Cont.

Model	Description
<b>SLR validation</b>	
Station coordinates	SLRF2014 [41]
Ocean tide loading	FES 2004 [36]
Tropospheric delay	Mendes and Pavlis [42]
Relativity	Space-time curvature correction

The flat-plate macro-model is widely adopted for the LEO mission and provides a proper tool to describe the non-gravitational force on the surfaces of a satellite [5,23,43]. The 13-plate macro-model obtained from [1] was used for HY-2B POD. The scale factors were taken into account for solar radiation pressure (SRP) and atmospheric drag force. The extended analytical SRP model developed by [39] was used, and photons in the visual (VIS) and infrared (IR) were considered in SRP. We assumed that 50% of the total solar radiation pressure is caused by shortwave and longwave radiations, and indicated this contribution as 1/2. The temporal variation in the solar radiation pressure can be ignored as it causes a very small effect [44]. The density values and composition data of the Earth's thermosphere obtained from DTM-2013 [40] were employed for a precise modeling of atmospheric forces. Moreover, empirical accelerations were introduced in POD solution to compensate for deficiencies of the modeled forces.

## 2.2. Frequency Characteristics

Non-gravitational modeling is challenging because it does not perfectly describe the real in-flight environment encountered by a spacecraft and often relies on a variety of external products [23,24,45]. In addition to the scaling parameter, a pre-defined number of empirical accelerations, such as piecewise periodic or constant accelerations, were applied to cope with the remaining deficiencies of the satellite's prior model [21,22]. Accordingly, the piecewise constant and periodic empirical accelerations can be obtained by:

$$\ddot{r} = a_0 + a_1 \cos(k \cdot v) + a_2 \sin(k \cdot v), \quad k = 1, 2, \dots \quad (1)$$

where  $\ddot{r}$  is the empirical acceleration used in POD,  $a_0$  is the constant acceleration,  $a_1$  and  $a_2$  are the coefficients of periodic acceleration, and  $k$  is the frequency of periodic acceleration. Based on a high-precision force model, the unmodeled dynamic model generally occurs at a frequency of one cycle per revolution (CPR) (i.e., 1 CPR empirical acceleration), which causes empirical acceleration, which is in the form of the orbital period [45]. For a refined PEA model, the fast Fourier transform (FFT) was used in this study to identify the potential periodicity of the satellite's empirical acceleration, and the frequency of PEA was reset for orbit determination and analysis.

To fulfill our aims, an optimized periodic PEA model was proposed and implemented for the HY-2B mission. The processing flow was roughly divided into two steps. First, the piecewise constant acceleration strategy (i.e., only a constant PEA is used in Formula (1)) was used in POD to obtain a priori information for the residual acceleration and an analysis of their spectra was performed to detect the potential periodic signals. Second, a frequency test was carried out for comparison and verification. The piecewise constant accelerations of HY-2B POD on Day 8 of the year 2019 are depicted in Figure 1, clearly indicating the time variability of the remaining accelerations. Note that the periodic signals of the PEA for three directions are generally difficult to identify (see Figure 1), and thus the FFT was used in this study.

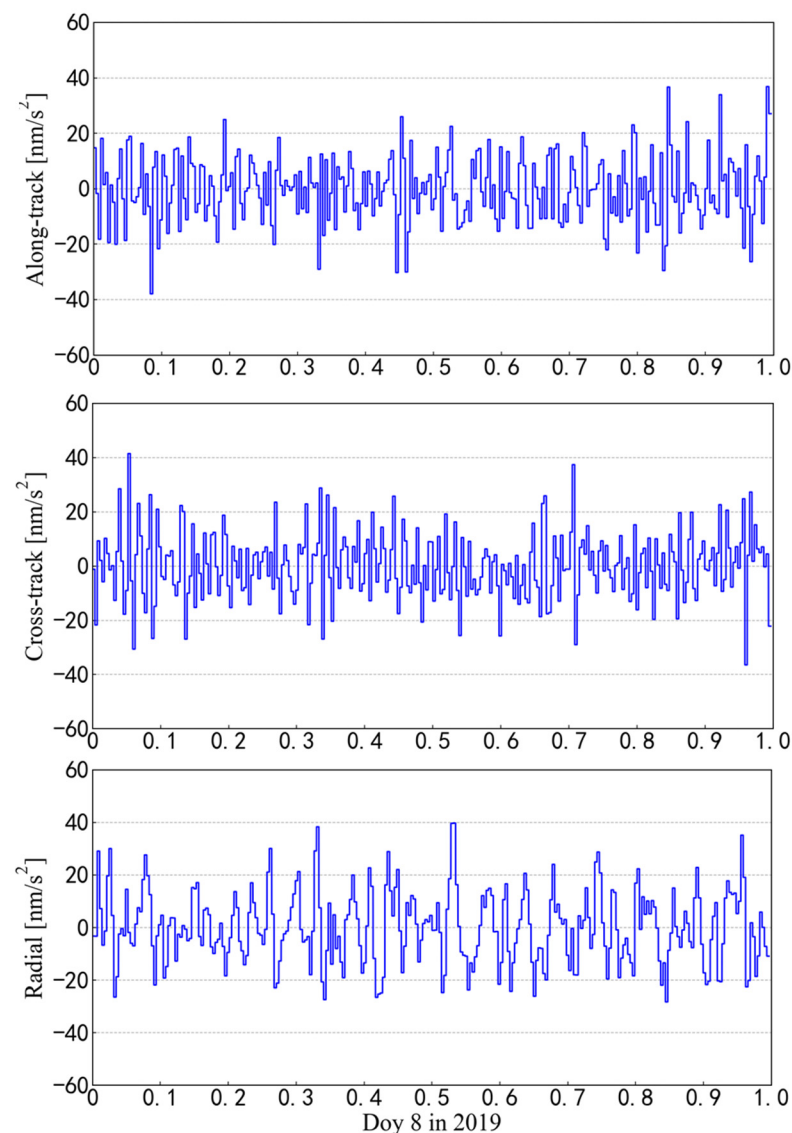


**Figure 1.** Piecewise constant accelerations of the reduced-dynamic orbit determination on 8 January 2019 (day of year DOY 8). These accelerations are described as constant values in the along-track (**top**), cross-track (**middle**), and radial (**bottom**) directions at consecutive intervals of 5 min.

As a starting point, estimated constant accelerations as well as reduced dynamic orbit solutions were obtained for a 14-day period, in which the acceleration value was used for spectral analysis. A power spectrum analysis of the residual accelerations in three directions is shown in Figure 2. The along-track direction and orbital radial direction show a clear periodic signal, while the results of the cross-track direction are complicated. For the along-track direction, 4 CPR is the dominant periodic signal. There is a noticeable signal of 2 CPR in the radial direction. However, a mixed spectrum is observed in the cross-track direction, and it is hard to identify the periodicity of the acceleration.

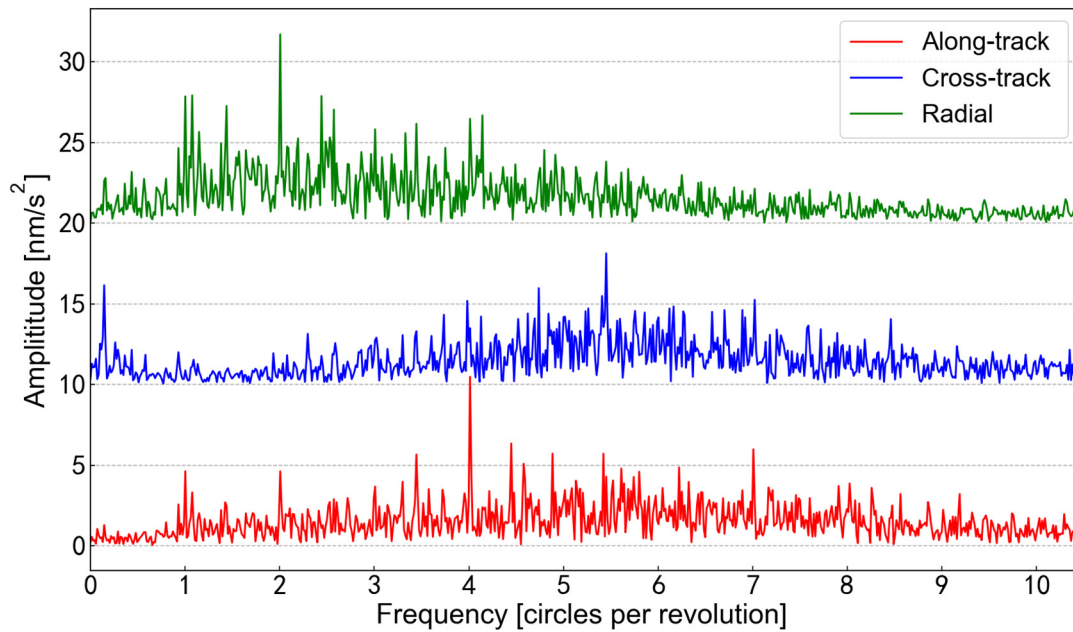


**Figure 2.** Amplitude spectrum of unmodeled accelerations in the along-track (red), cross-track (blue), and radial (green) directions. Values for the cross-track and radial directions are shifted by +10 nm/s<sup>2</sup> and +20 nm/s<sup>2</sup>, respectively.

### 2.3. Refined PEA Model of HY-2B

Figure 2 shows the presence of a low-frequency signal and a 5.5 CPR signal, and the power spectrum magnitudes of the two signals are almost equivalent. Due to the existence of high- and low-frequency signals, it may be necessary to make the empirical acceleration in the cross-track direction in the form of a combination of constant and periodic signals. Moreover, the conventional 1 CPR signal in the cross-track direction can be considered as a comprehensive scheme. Based on these results, the PEA models of the empirical acceleration in the along-track and normal directions can be obtained as:

$$\begin{aligned} \ddot{r}_A &= a_1 \cos(k \cdot v) + a_2 \sin(k \cdot v), \quad k = 4 \\ \ddot{r}_c &= a_0 + a_1 \cos(k \cdot v) + a_2 \sin(k \cdot v), \quad k = 5.5 \end{aligned} \quad (2)$$

and:

$$\begin{aligned} \ddot{r}_A &= a_1 \cos(k \cdot v) + a_2 \sin(k \cdot v), \quad k = 4 \\ \ddot{r}_C &= a_1 \cos(k \cdot v) + a_2 \sin(k \cdot v), \quad k = 1 \end{aligned} \quad (3)$$

Likewise, the individual empirical accelerations in three directions can be expressed as:

$$\begin{aligned} \ddot{r}_A &= a_1 \cos(k \cdot v) + a_2 \sin(k \cdot v), \quad k = 4 \\ \ddot{r}_c &= a_0 + a_1 \cos(k \cdot v) + a_2 \sin(k \cdot v), \quad k = 5.5 \\ \ddot{r}_R &= a_1 \cos(k \cdot v) + a_2 \sin(k \cdot v), \quad k = 2 \end{aligned} \quad (4)$$

and

$$\begin{aligned} \ddot{r}_A &= a_1 \cos(k \cdot v) + a_2 \sin(k \cdot v), \quad k = 4 \\ \ddot{r}_C &= a_1 \cos(k \cdot v) + a_2 \sin(k \cdot v), \quad k = 1 \\ \ddot{r}_R &= a_1 \cos(k \cdot v) + a_2 \sin(k \cdot v), \quad k = 2 \end{aligned} \quad (5)$$

The periodic term of the empirical acceleration in three directions defined by the local orbital reference frame has been revealed, and the power spectrum of the cross-track direction is worth discussing. The spectrum results show that there are two differences between the normal direction and the other two directions. The power spectrum's amplitude of acceleration in the normal direction is smaller than that in the along-track and radial directions, which is related to the magnitude of acceleration and the intensity of the signal. On the other hand, there is no obvious dominant signal in the normal direction, and there are

coexisting high- and low-frequency signals. The optimal frequency combination for PEA is discussed in the following section, and a refined PEA combination can independently be inferred from the SLR validation.

### 3. Improvements in HY-2B POD

Based on the processing standards described in Section 2.3, assessments of each processing chain are described in this section. In addition to satellite dynamics, improving the geometric strength is a powerful means of improving the orbital accuracy of LEO satellites. GPS antenna offset calibration and an assessment of single-receiver ambiguity resolution were performed for the HY-2B satellites, as we describe in this section. An internal consistency analysis and external validations are provided for different orbit solutions. The GPS data covering the period since the initial GPS receiver operation (November 2018) to the end of 2019 were used.

#### 3.1. Performance Analysis of the Refined PEA Model

For a clear identification, a unique identifier (ID) was introduced based on the processing strategy described in Section 2.3. The solution IDs consider the differences in the direction and frequency of PEA (see Table 2). The first digit in the code represents the along-track direction, the second digit represents the cross-track direction, and the third digit is the radial direction. The number represents the frequency of empirical acceleration in that direction. For example, the 111 solution means that the empirical acceleration is set at 1 CPR in all three directions, whereas the 110 solution means that the empirical acceleration is set at 1 CPR in the along-track and cross-track directions. The letter “C” in 110 + C represents the addition of constant acceleration in the cross-track direction to the 110 solution. To facilitate the identification, the 5.5 CPR signal is referred to as a 6 CPR signal (see Table 2). In addition to the strategies mentioned in Section 2.2, the 110 and 111 solutions were used as regular strategies for comparison.

**Table 2.** Three-digit codes for different PEA solutions in POD. The number represents the frequency of periodic acceleration, and the letter ‘C’ represents the addition of constant acceleration in the cross-track direction.

Solution Type	Along-Track		Cross-Track		Radial	
	Periodic Acc.	Constant Acc.	Periodic Acc.	Constant Acc.	Periodic Acc.	Constant Acc.
110	1 CPR	No	1 CPR	No	No	No
410	4 CPR	No	1 CPR	No	No	No
460 + C	4 CPR	No	5.5 CPR	Yes	No	No
111	1 CPR	No	1 CPR	No	1 CPR	No
412	4 CPR	No	1 CPR	No	2 CPR	No
462 + C	4 CPR	No	5.5 CPR	Yes	2 CPR	No

Spectral analysis of the unmodeled acceleration provides effective prior information for setting the frequency of the periodic PEA. The approach taken to optimize the PEA model was to change the perturbation frequency to improve the orbit’s accuracy. A frequency test based on spectral analysis was used to verify whether better orbit determination results could be obtained when the empirical acceleration was consistent with the characteristic signal of the spectrum results. The SLR technique is a powerful means of evaluating a GPS-based orbit [46] and it was used to evaluate the orbit accuracy of the PEA model with different solutions. The fitting curve of the SLR residual with elevation angle and azimuth angle was used [47,48]. Eleven high-performance International Laser Ranging Service (ILRS) stations (i.e., Yarragadee (7090), Greenbelt (7105), Haleakala (7119), Hartebeest (7501), Zimmerwald (7810), Mt. Stromlo (7825), Graz (7839), Herstmonceux

(7840), Potsdam (7841), Matera (7941), and Wettzel (8834)) [46] were used for SLR validation. The relevant models used in processing are listed in Table 1.

The trend line for all stations' SLR residuals with respect to the elevation angle (see Figure 3) showed an overall dependency on the orbit solutions. The SLR residuals from the 110 orbit solution showed high dependency; much lower mean residuals were found for Solutions 410 and 460 + C. The 410 or 460 + C solutions probably represent reality well. It is worth mentioning that the empirical accelerations in the along-track direction compensated for the effect of the unmodeled part of the atmospheric drag. Both models deal with non-conservative forces in the along-track direction, and thus there is a process of mutual influence. The dependency between the SLR residuals and the azimuth angles from the stations to the satellite is shown in Figure 4. A large mean bias occurred for the 111 and 412 solutions, and a slight improvement was observed for the 462 + C solution.

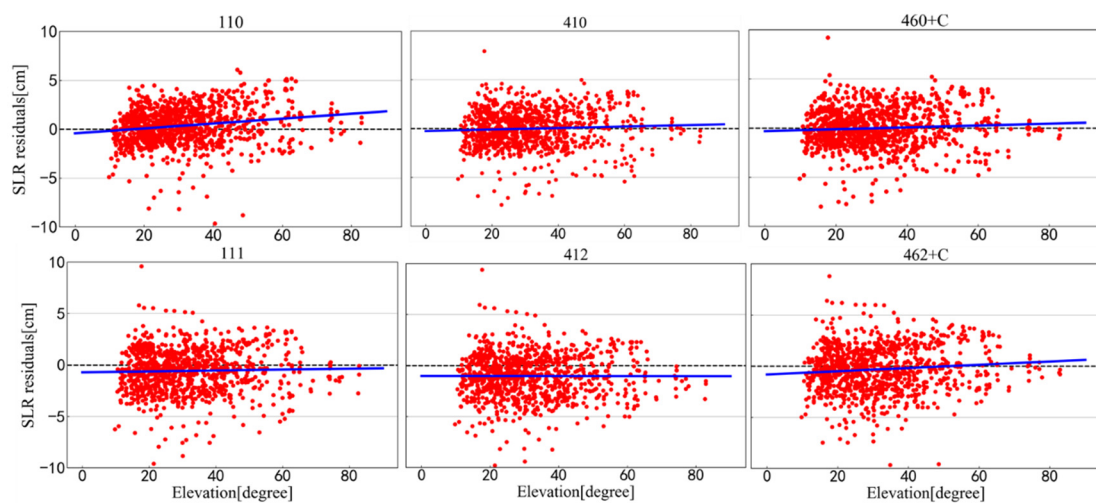


**Figure 3.** SLR residuals (red dot) with respect to the elevation angle for all sites, with a trend line (blue). All six PEA solutions are displayed for comparison.

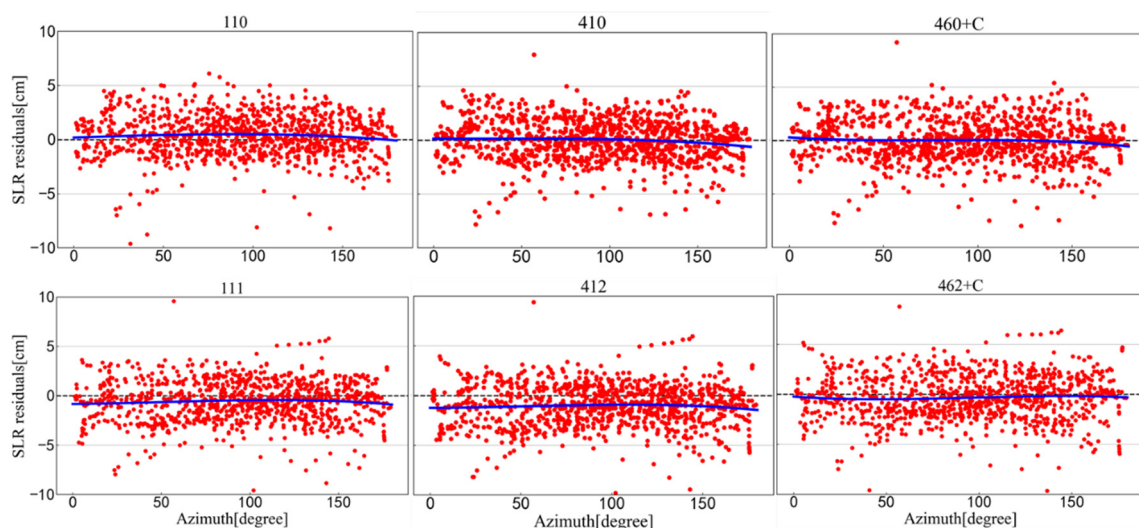


**Figure 4.** SLR residuals (red dot) obtained for the six PEA solutions with respect to the azimuth angle for all sites. A trend line (blue) is fitted with polynomials.

An overview of SLR validation of the different PEA solutions over a 14-day dataset is shown in Table 3. In general, the 410 orbit solution was the best for SLR validation, and the 460 + C solution closely agreed with the spectral characteristics of acceleration. The

SLR validation of this strategy was slightly worse than that of the 410 solution but it still achieved good accuracy. The SLR validation (see Table 3) showed that the 110 solution, which only estimated the acceleration in the along-track and cross-track directions, achieved the expected orbit determination accuracy. The radial direction of LEO satellites is mainly affected by conservative forces such as the gravitational field and tidal perturbation of the Earth; it is also affected by Earth radiation pressure, which results in a slight and constant acceleration. Considering the weak performance of the solutions with estimation of the radial acceleration, the related solutions (i.e., 111, 412, and 462 + C) were not used in the reprocessing of HY-2B POD.

**Table 3.** SLR residuals of different PEA strategies in POD. The SLR measurements were obtained from 11 individual ILRS stations and used in validations of the HY-2B orbit.

PEA Solution	Mean (mm)	RMS (mm)	Note
110	2.6	16.6	r
410	−1.5	15.7	r
460 + C	−2.0	16.5	r
111	−4.4	18.1	
412	−5.4	18.5	
462 + C	−2.1	17.5	

Note: “r” means that the PEA solution was used in the reprocessing of HY-2B POD.

Based on the spectral analysis of HY-2B empirical accelerations and orbit validation, the reprocessing arc was extended from 1 November 2018 to 1 January 2020, and three different PEA strategies were used in reprocessing (see Table 3). The SLR validation of the reprocessing of HY-2B POD is shown in Figure 5. The 110 solution participated in reprocessing as a routine strategy, while the remaining two strategies, i.e., the 410 and 460 + C solutions, performed well in the frequency test. Compared with the 110 solution, the 410 solution provided better SLR validation after changing the frequency of the along-track direction. The SLR residuals of the 11 high-performance SLR stations were improved to some extent.

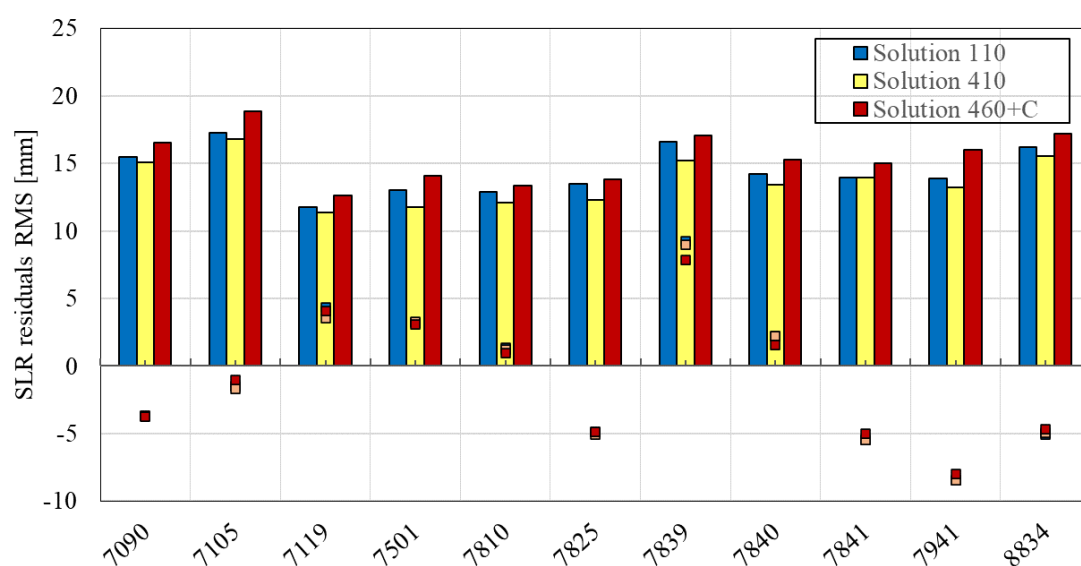


**Figure 5.** Statistics of the SLR residuals for individual SLR sites for three reprocessing strategies. The square is mean bias for each contributing station.

According to the SLR validation for the different PEA solutions over 14 months of the HY-2B mission, an optimized PEA strategy can be suggested. The 410 solution appeared to be the best among the three strategies in terms of SLR validation: the RMS of the SLR residuals of the 410 solution was 5.23% better than that of the 110 solution. When the frequency of the along-track direction was kept at 4 CPR, the result of the 460 + C solution with constant and periodic signals in the normal direction was slightly worse than that of the 110 solution. The 460 + C solution was the worst among those analyzed, but the average value of the SLR validation was slightly improved. For the mixed spectrum of the cross-track direction, 1 CPR as a comprehensive solution could deal with this situation well, and the validation using SLR observations proved this point.

### 3.2. GPS Antenna Offset Calibration

For a high-quality determination of the LEO orbit, the additional in-flight calibration of the LEO GPS antenna is essential [25,49]; the impact of unmodeled systematic errors on the HY-2B orbit is discussed. The validity of the GPS receiver antenna phase center for the HY-2B and a correction value are assessed in this section. The generation of the HY-2B GPS antenna phase center's location was based on the PCO vectors, (e.g., from the ground calibration), and no additional PCO was provided. As a starting point, the reduced-dynamic POD as well as an estimation of the PCO's z-component (i.e., the direction of the upward-facing antenna's boresight) were obtained for a 420-day period. A 20 mm systematic discrepancy in the modeled antenna phase center could be observed for the HY-2B (see Table 4). A 20 mm correction in the PCO z-component was adopted for further study, and the phase residual from POD was obviously improved, as shown in Figure 6. The negative residuals in the low-elevation area near the azimuth ( $0^\circ$  and  $180^\circ$ ) were significantly reduced; Figure 6 shows a typical example for this situation.

**Table 4.** Coordinates for the GPS receiver and CoM in the body-fixed coordinate system.

Item	Reference (x, y, z) (mm)	Notes
CoM location	(+1332.000, −8.600, +3.400)	Nov. 2018
GPS antenna location	(+347.290, −175.140, −1372.680)	Main antenna (GPS a)
GPS antenna PCO	(+0.0, +0.0, +20.0)	Estimated PCO-offset valid for ionosphere-free L1/L2

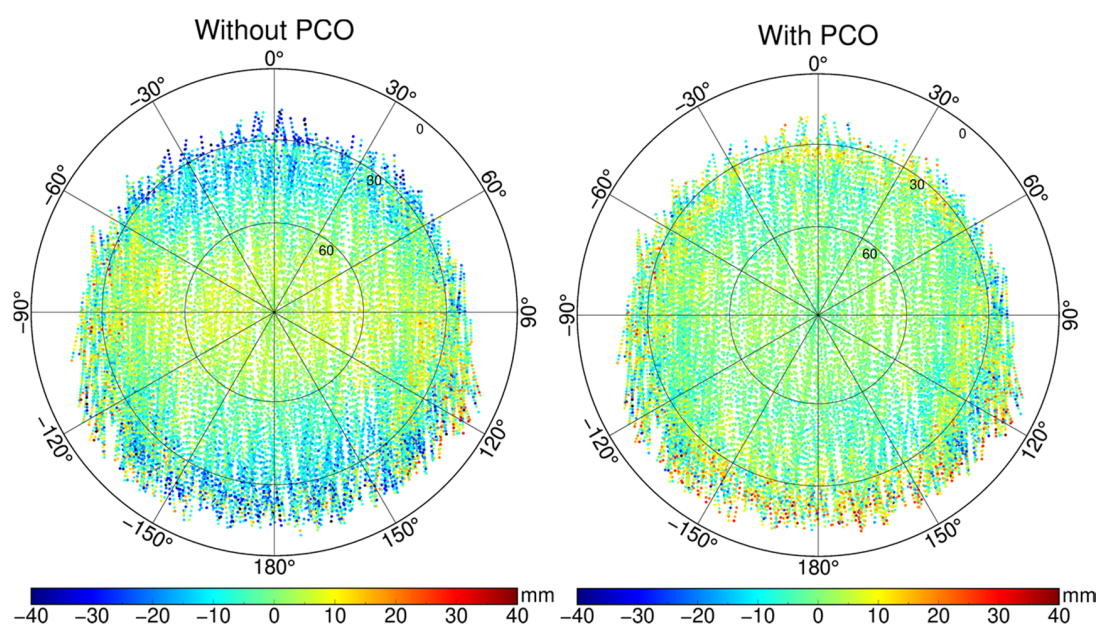


**Figure 6.** Sky plot of the residuals of the ionosphere-free L1/L2 carrier phase combination for HY-2B on 1 January 2019. The azimuth  $0^\circ$  of the antenna frame coincides with the +x-axis of the spacecraft's body, which points into the flight direction.

The residual approach [25,50] was used to obtain the phase map (see Figure 7) from the ionosphere-free carrier phase residuals over a 420-day data span. The PCV map describes the empirical phase pattern corrections around the given phase center. The static multipath or other near-field effects caused by satellite components near the GPS antenna are potential sources of these variations. Similar to other missions, flight calibration for the GPS antenna and estimation of the PCV map from actual observations have been a standard practice for POD [16,26,49].

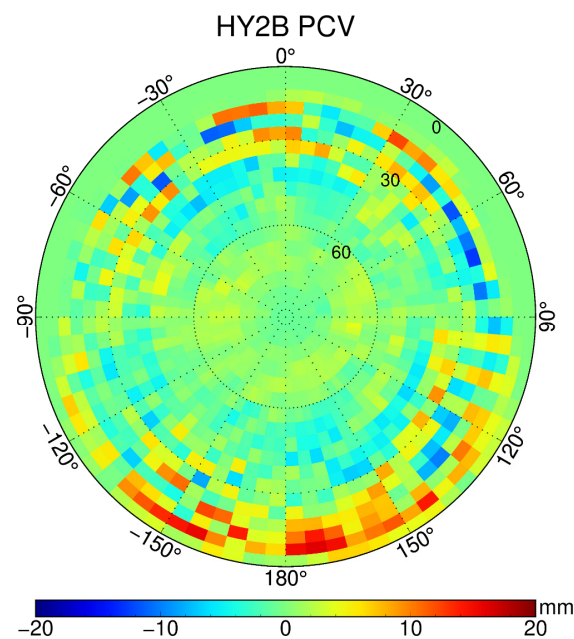


**Figure 7.** Estimated azimuth elevation diagrams of the  $5^\circ \times 5^\circ$  PCV patterns for the HY-2B satellite.

Considering fuel loss and deformation caused by in-flight temperature variations, a long-term analysis of the locations of the GPS antenna phase center was carried out. Table 4 shows the average value of the PCO z-component estimation, and the change in daily estimation is discussed (see Figure 8). The offset deviation of the PCO z-component fluctuated by about 21 mm since the start of the mission, while its offset changed by around 18 mm one year after the launch. The trend of 2–3 mm in the z-direction can be observed in Figure 8. Regular updates of the PCO of onboard receivers are indispensable to ensure high-precision orbit determination.

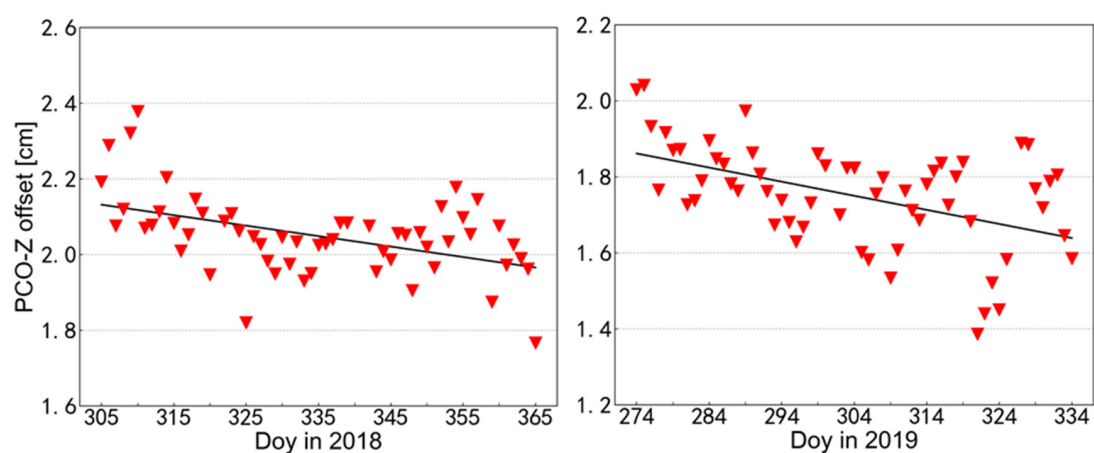


**Figure 8.** Estimation of the PCO z-component (red triangle) for HY-2B at the beginning of the satellite's mission (left) and one year later (right). The black line is the trend line fitted by least squares.

For an assessment of the HY-2B POD solutions with PCO/PCV correction, the uncorrected and newly corrected orbits were compared against the SLR observations. Figure 9 shows the SLR residuals of the two orbit solutions from 11 high-performance stations. It is clear that the PCO/PCV correction improved the overall accuracy of the POD solution for HY-2B. SLR validation demonstrated a 26% improvement for the orbit solution with PCO/PCV correction, and a 1.57 cm RMS of SLR residuals for the reduced-dynamic orbits was obtained. This means that the HY-2B POD product is of high quality, which is extremely important for an altimetry satellite.

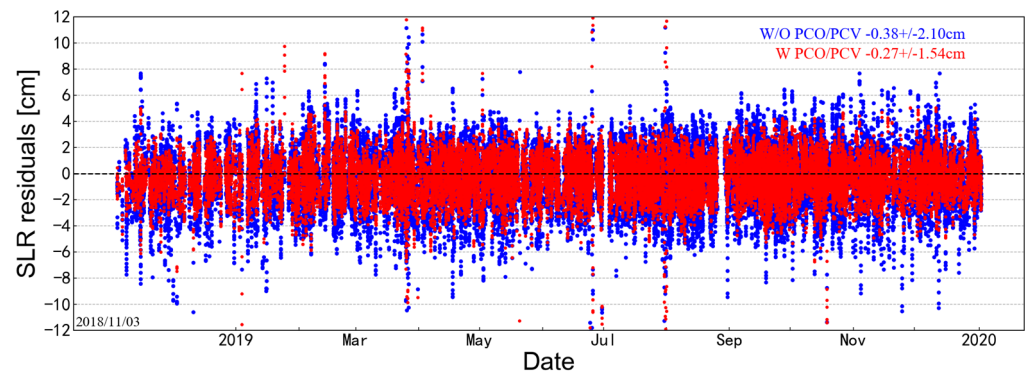


**Figure 9.** SLR residuals for HY-2B precise orbit determination using the nominal phase center (blue dot) and PCO/PCV correction (red dot) over a 14-month period.

### 3.3. Single-Receiver Ambiguity Resolution

Reprocessing of the raw GPS data from the HY-2B satellite covering the period from the launch (11 November 2018) to end of 2019 was performed for this study to support single-receiver ambiguity resolution. The CNES-CLS wide-lane satellite bias (WSB) product, complementary to these biases, and the CNES-CLS clock product were used in the GPS-based precise orbit determination. Details of this process and successful implementation of the Swarm GPS receiver and the Sentinel-3 GPS receiver are described in [16,29].

Over the 1-year timeframe displayed in Figure 10, average fixed rates of 92.19% for wide-lane ambiguities and 73.93% for narrow-lane ambiguities were obtained for HY-2B. Simple integer rounding is sufficient in practice to solve the mixed-integer problem [16,20], and the acceptance criterion of 0.24 and 0.12 cycles, respectively, was used. No notable variations in the success rate for wide-lane and narrow-lane ambiguity fixing could be recognized.

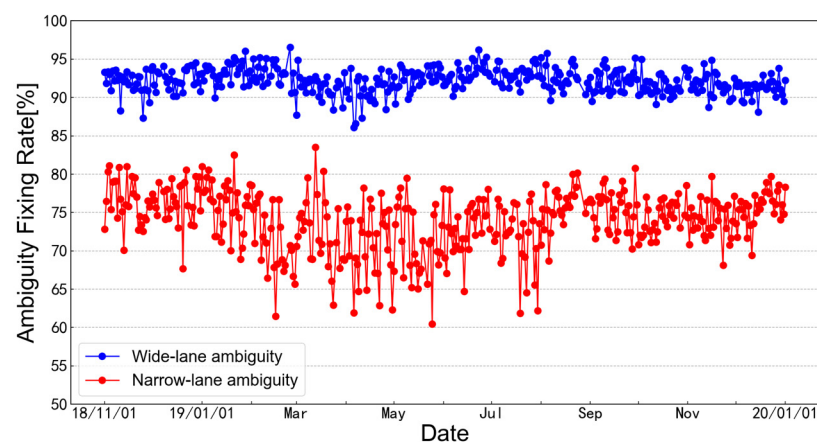


**Figure 10.** Fraction of passes with resolved wide-lane and narrow-lane ambiguities for the HY-2B satellite from November 2018 to the end of 2019.

SLR measurements are used as a totally independent technique to evaluate the accuracy of GPS-based orbits for the HY-2B satellite. RMS SLR residuals of 15.7 and 13.3 mm were obtained for the float ambiguity (FA) solution and the ambiguity-fixed (AF) solution, respectively (see Table 5). The overall reduction of 15.3% in the RMS SLR residuals proved that AF POD solutions are a powerful strategy for improving orbit accuracy. A well-established SLR validation depends heavily on the station coordinates and station-specific ranging biases [7,51]. For a better interpretation, the mean and standard deviation of the SLR residuals for each ILRS station are presented in Table 5. An overall mean bias of about 2 mm was found in the SLR validation. In all computations, observations above the 8° elevation were employed, and an outlier threshold of 15 cm (only 0.88% of the SLR data were rejected) was applied.

**Table 5.** SLR residuals and number of normal points for 11 high-performance ILRS stations used for the validation of the HY-2B orbit.

Station (ID)	$N_{np}$	Float Amb.		Amb. Fixed	
		Mean (mm)	STD (mm)	Mean (mm)	STD (mm)
Yarragadee (7090)	10,496	−3.3	16.0	−3.3	13.7
Greenbelt (7105)	3102	−4.2	17.3	−4.0	14.8
Haleakala (7119)	1010	3.2	11.8	3.3	10.2
Hartebeest (7501)	2265	3.4	15.6	1.9	11.3
Zimmerwald (7810)	3990	−0.4	12.4	−1.1	10.2
Mt. Stromlo (7825)	5447	−5.1	13.3	−5.5	9.9
Graz (7839)	2224	7.2	16.2	6.2	13.7
Herstmonceux (7840)	2726	−0.2	13.8	−1.4	12.2
Potsdam (7841)	1212	−8.8	13.6	−9.3	11.7
Matera (7941)	2024	−9.8	13.8	−9.7	11.4
Wetzels (8834)	1730	−8.2	17.5	−8.8	13.7
Total	36,226	−2.3	15.7	−2.7	13.3

#### 4. Discussion

In this paper, the refined PEA strategy is proposed for superior orbital accuracy of the HY-2B satellite. A spectral analysis was performed to identify the potential periodicity of empirical acceleration in HY-2B POD. Noticeable signals were identified in the along-track and radial directions, and a mixed spectrum was observed for the cross-track direction. According to the spectral analysis of HY-2B empirical accelerations, six sets of PEA strategies were employed to assess the impact of the PEA model on the POD performance. SLR, as a completely independent space-geodetic technology, was used to evaluate the accuracy of GPS-based orbit solutions [46,52]. In order to deal with the complexity of the cross-track direction, two comprehensive PEA strategies were adopted for HY2B POD. Moreover, we found that the PEA model with empirical parameters in the along-track and cross-track directions provided satisfying orbit determination accuracy. This indicates that the forces in the radial direction of the satellite were well described by the background model. The 14 months of GPS observations are used for the reprocessing to evaluate different PEA solutions. It is worth mentioning that the optimized PEA strategy in this article is only applicable to HY2B satellites. Future work can consider investigating the POD performance of the refined PEA model for other LEO satellites and can also focus on the refinement of non-gravitational force modeling that might further reduce the uncertainty in LEO POD [13,20,24].

Similar to other LEO missions, inconsistencies at a level of 2 cm were confirmed for the HY-2B GPS antenna phase center [16,25,26]. More than one year's data were used for PCO estimation, and the change trend in the PCO z-component could be inferred from the time series of the results. The GRG provided by the CNES/CLS analysis center was used to support the implementation of HY-2B ambiguity-fixed POD solutions, which resulted in a 15% improvement of SLR residuals compared to the float solution. Similar results based on OBS-based products provided by CODE were also obtained by other LEO satellite missions [13,30]. The improvement of these GNSS products will benefit the LEO POD community.

## 5. Conclusions

A set of improved orbit solutions covering a period of more than a year was generated for the HY-2B satellite using a refined dynamic modeling and processing strategy. Key enhancements focused on a refined PEA strategy, GPS receiver offset calibration, and the implementation of integer ambiguity resolution. Updates to each processing strategy resulted in varying degrees of improvement for the orbit. Normally, PEA is used to absorb the uncertainties of physical modelling. To better understand the time-varying residual acceleration of spacecraft, here, we presented a refined PEA model. A spectral analysis was conducted to identify the potential periodicity of empirical acceleration in the HY-2B POD, and the main signals existing in the three dimensions (along-track, cross-track, and radial direction) were extracted and analyzed. The 4 CPR signal in the along-track direction and the 2 CPR in the radial direction were identified, and a mixed spectrum was observed for the cross-track direction. The three reprocessing strategies were applied to select an orbit solution of high quality. In the SLR validation, the refined PEA model with 4 CPR periodic acceleration in the along-track direction and 1 CPR periodic acceleration in the cross-track direction allowed a comprehensive strategy that could deal well with the mixed spectrum in the cross-track direction. Compared with regular strategies, a noticeable improvement in the SLR residuals for high-grade SLR stations was possible for orbits using the refined PEA strategy, which is still suggested as an ideal strategy for empirical acceleration modeling.

Estimation of the PCO and modeling of the PCV can effectively eliminate the systematic deviation related to signal incidence and significantly reduce the phase residuals. A systematic bias of 20 mm for the HY-2B GPS antenna phase center could be observed. Based on the PCO's z-component time series of more than 1 year, a decreasing trend appeared in this direction. For 11 high-performance SLR sites, SLR residuals with a standard deviation as low as 15.7 mm were obtained for the HY-2B POD, which produced a 25% improvement compared with the solution without PCO/PCV. Ambiguity resolution added a strong constrained geometry for other estimation parameters in POD, and better orbit precision (13.3 mm RMS) was confirmed by independent SLR measurements. Some studies related to ours are available [13,16,53]. The lean set of auxiliary data from the CNES/CLS products will be attractive for the wider LEO POD community.

**Author Contributions:** Conceptualization, Y.W. and M.L. (Min Li); methodology, Y.W. and K.J.; software, M.L. (Min Li) and Q.Z.; validation, K.J., W.L. and G.Q.; formal analysis, M.L. (Min Li); investigation, Y.W. and K.J.; resources, H.P. and M.L. (Mingsen Li); data curation, Y.W. and M.L. (Min Li); writing—original draft preparation, Y.W.; writing—review and editing, M.L. (Min Li); visualization, Y.W.; supervision, M.L. (Min Li); project administration, M.L. (Mingsen Li) and H.P.; funding acquisition, M.L. (Min Li). All authors have read and agreed to the published version of the manuscript.

**Funding:** This study was supported by the National Natural Science Foundation of China (Grant Nos. 42074032, 41931075, 42030109 and 42004020) and the Wuhan Science and Technology Bureau (2019010701011391).

**Data Availability Statement:** The GNSS precise orbit and clock products are publicly available from <ftp://igs.gnsswhu.cn/pub/gnss/products/mgex/> (accessed on 1 August 2021). The SLR observations of HY-2B is provided by ILRS at <ftp://cddis.gsfc.nasa.gov/pub/slr/data/> (accessed on 1 August 2021). The SLRF2014 station coordinates is obtained from <ftp://gdc.cddis.eosdis.nasa.gov/pub/slr/products/resource/> (accessed on 1 August 2021). The data that support this study are available from the corresponding author upon reasonable request.

**Acknowledgments:** We are grateful to the IGS for providing the GNSS products and to the ILRS for providing the SLR observations of the HY-2B satellite.

**Conflicts of Interest:** The authors declare no conflict of interest.

## References

1. NSOAS. HY-2: A Marine Remote Sensing Satellite Series Planned by China. 2021. Available online: <http://www.nsoas.org.cn/index.html> (accessed on 1 August 2021).
2. Rudenko, S.; Neumayer, K.H.; Dettmering, D.; Esselborn, S.; Schone, T.; Raimondo, J.C. Improvements in Precise Orbits of Altimetry Satellites and Their Impact on Mean Sea Level Monitoring. *IEEE Trans. Geosci. Remote Sens.* **2017**, *55*, 3382–3395. [[CrossRef](#)]
3. Hackel, S.; Gisinger, C.; Balss, U.; Wermuth, M.; Montenbruck, O. Long-Term Validation of TerraSAR-X and TanDEM-X Orbit Solutions with Laser and Radar Measurements. *Remote Sens.* **2018**, *10*, 762. [[CrossRef](#)]
4. Zhang, Q.; Guo, X.; Qu, L.Z.; Zhao, Q.L. Precise Orbit Determination of FY-3C with Calibration of Orbit Biases in BeiDou GEO Satellites. *Remote Sens.* **2018**, *10*, 382. [[CrossRef](#)]
5. Tapley, B.D.; Ries, J.C.; Davis, G.W.; Eanes, R.J.; Schutz, B.E.; Shum, C.K.; Watkins, M.M.; Marshall, J.A.; Nerem, R.S.; Putney, B.H.; et al. Precision Orbit Determination for Topex/Poseidon. *J. Geophys. Res.-Oceans* **1994**, *99*, 24383–24404. [[CrossRef](#)]
6. Flohrer, C.; Otten, M.; Springer, T.; Dow, J. Generating precise and homogeneous orbits for Jason-1 and Jason-2. *Adv. Space Res.* **2011**, *48*, 152–172. [[CrossRef](#)]
7. Arnold, D.; Montenbruck, O.; Hackel, S.; Sośnica, K. Satellite laser ranging to low Earth orbiters: Orbit and network validation. *J. Geod.* **2018**, *93*, 2315–2334. [[CrossRef](#)]
8. Strugarek, D.; Sosnica, K.; Arnold, D.; Jäggi, A.; Zajdel, R.; Bury, G.; Drozdowski, M. Determination of Global Geodetic Parameters Using Satellite Laser Ranging Measurements to Sentinel-3 Satellites. *Remote Sens.* **2019**, *11*, 2282. [[CrossRef](#)]
9. Wang, Y.C.; Guo, J.Y.; Zhou, M.S.; Jin, X.; Zhao, C.M.; Chang, X.T. Geometric solution method of SLR station coordinate based on multi-LEO satellites. *Chin. J. Geophys.* **2020**, *63*, 4333–4344. [[CrossRef](#)]
10. Wu, S.C.; Yunck, T.P.; Thornton, C.L. Reduced-dynamic technique for precise orbit determination of low earth satellites. *J. Guid. Control Dyn.* **1991**, *14*, 24–30. [[CrossRef](#)]
11. Li, M.; Li, W.W.; Shi, C.; Jiang, K.C.; Guo, X.; Dai, X.L.; Meng, X.G.; Yang, Z.D.; Yang, G.L.; Liao, M. Precise orbit determination of the Fengyun-3C satellite using onboard GPS and BDS observations. *J. Geod.* **2017**, *91*, 1313–1327. [[CrossRef](#)]
12. Kornfeld, R.P.; Arnold, B.W.; Gross, M.A.; Dahya, N.T.; Klipstein, W.M.; Gath, P.F.; Bettadpur, S. GRACE-FO: The Gravity Recovery and Climate Experiment Follow-On Mission. *J. Spacecr. Rocket.* **2019**, *56*, 931–951. [[CrossRef](#)]
13. Mao, X.; Arnold, D.; Girardin, V.; Villiger, A.; Jäggi, A. Dynamic GPS-based LEO orbit determination with 1 cm precision using the Bernese GNSS Software. *Adv. Space Res.* **2021**, *67*, 788–805. [[CrossRef](#)]
14. Montenbruck, O.; van Helleputte, T.; Kroes, R.; Gill, E. Reduced dynamic orbit determination using GPS code and carrier measurements. *Aerosp. Sci. Technol.* **2005**, *9*, 261–271. [[CrossRef](#)]
15. Jiang, K.C.; Li, M.; Wang, M.; Zhao, Q.L.; Li, W.W. TJS-2 geostationary satellite orbit determination using onboard GPS measurements. *GPS Solut.* **2018**, *22*, 87. [[CrossRef](#)]
16. Montenbruck, O.; Hackel, S.; Jäggi, A. Precise orbit determination of the Sentinel-3A altimetry satellite using ambiguity-fixed GPS carrier phase observations. *J. Geod.* **2018**, *92*, 711–726. [[CrossRef](#)]
17. Kang, Z.; Tapley, B.; Bettadpur, S.; Ries, J.; Nagel, P.; Pastor, R. Precise orbit determination for the GRACE mission using only GPS data. *J. Geod.* **2006**, *80*, 322–331. [[CrossRef](#)]
18. Bock, H.; Jäggi, A.; Beutler, G.; Meyer, U. GOCE: Precise orbit determination for the entire mission. *J. Geod.* **2014**, *88*, 1047–1060. [[CrossRef](#)]
19. Van den Ijssel, J.; Encarnação, J.; Doornbos, E.; Visser, P. Precise science orbits for the Swarm satellite constellation. *Adv. Space Res.* **2015**, *56*, 1042–1055. [[CrossRef](#)]
20. Montenbruck, O.; Hackel, S.; van den Ijssel, J.; Arnold, D. Reduced dynamic and kinematic precise orbit determination for the Swarm mission from 4 years of GPS tracking. *GPS Solut.* **2018**, *22*, 79. [[CrossRef](#)]
21. Švehla, D.; Rothacher, M. Kinematic and reduced-dynamic precise orbit determination of low earth orbiters. *Adv. Geosci.* **2003**, *1*, 47–56. [[CrossRef](#)]
22. Jäggi, A.; Hugentobler, U.; Beutler, G. Pseudo-Stochastic Orbit Modeling Techniques for Low-Earth Orbiters. *J. Geod.* **2006**, *80*, 47–60. [[CrossRef](#)]
23. Hackel, S.; Montenbruck, O.; Steigenberger, P.; Balss, U.; Gisinger, C.; Eineder, M. Model improvements and validation of TerraSAR-X precise orbit determination. *J. Geod.* **2016**, *91*, 547–562. [[CrossRef](#)]

24. Hackel, S. *Refinement of Reduced-Dynamic Orbit Determination for Low Earth Satellites*; Technische Universität München: Munich, Germany, 2019.
25. Jäggi, A.; Dach, R.; Montenbruck, O.; Hugentobler, U.; Bock, H.; Beutler, G. Phase center modeling for LEO GPS receiver antennas and its impact on precise orbit determination. *J. Geod.* **2009**, *83*, 1145–1162. [[CrossRef](#)]
26. Lu, C.X.; Zhang, Q.; Zhang, K.K.; Zhu, Y.T.; Zhang, W. Improving LEO precise orbit determination with BDS PCV calibration. *GPS Solut.* **2019**, *23*, 109. [[CrossRef](#)]
27. Visser, P.N.A.M.; van den Ijssel, J.A.A. Calibration and validation of individual GOCE accelerometers by precise orbit determination. *J. Geod.* **2015**, *90*, 1–13. [[CrossRef](#)]
28. Peter, H.; Jäggi, A.; Fernández, J.; Escobar, D.; Ayuga, F.; Arnold, D.; Wermuth, M.; Hackel, S.; Otten, M.; Simons, W.; et al. Sentinel-1A—First precise orbit determination results. *Adv. Space Res.* **2017**, *60*, 879–892. [[CrossRef](#)]
29. Laurichesse, D.; Mercier, F.; Berthias, J.P.; Broca, P.; Cerri, L. Integer ambiguity resolution on undifferenced GPS phase measurements and its application to PPP and satellite precise orbit determination. *Navigation* **2009**, *56*, 135–149. [[CrossRef](#)]
30. Schaer, S.; Villiger, A.; Arnold, D.; Dach, R.; Prange, L.; Jäggi, A. The CODE ambiguity-fixed clock and phase bias analysis products: Generation, properties, and performance. *J. Geod.* **2021**, *95*, 81. [[CrossRef](#)]
31. Loyer, S.; Perosanz, F.; Mercier, F.; Capdeville, H.; Marty, J.-C. Zero-difference GPS ambiguity resolution at CNES–CLS IGS Analysis Center. *J. Geod.* **2012**, *86*, 991–1003. [[CrossRef](#)]
32. Reischung, P.; Schmid, R. IGS14/igs14.atx: A new framework for the IGS products. In Proceedings of the AGU Fall Meeting Abstracts, San Francisco, CA, USA, 12–16 December 2016.
33. Schmid, R.; Dach, R.; Collilieux, X.; Jäggi, A.; Schmitz, M.; Dilssner, F. Absolute IGS antenna phase center model igs08.atx: Status and potential improvements. *J. Geod.* **2016**, *90*, 343–364. [[CrossRef](#)]
34. Shako, R.; Förste, C.; Abrikosov, O.; Bruinsma, S.; Marty, J.-C.; Lemoine, J.-M.; Flechtner, F.; Neumayer, H.; Dahle, C. EIGEN-6C: A High-Resolution Global Gravity Combination Model Including GOCE Data. In *Observation of the System Earth from Space—Champ, Grace, Goce and Future Missions*; Flechtner, F., Sneeuw, N., Schuh, W.-D., Eds.; Advanced Technologies in Earth Sciences; Springer: Berlin/Heidelberg, Germany, 2014; pp. 155–161.
35. Petit, G.; Luzum, B. *IERS Conventions*; Bureau International des Poids et Mesures: Sevres, France, 2010.
36. Lyard, F.; Lefevre, F.; Letellier, T.; Francis, O. Modelling the global ocean tides: Modern insights from FES2004. *Ocean Dyn.* **2006**, *56*, 394–415. [[CrossRef](#)]
37. Standish, E.M. JPL Planetary and Lunar Ephemerides, DE405/LE405. Interoffice Memorandum: JPL IOM 312.F-98-048, 1998, August 26. Available online: <ftp://ssd.jpl.nasa.gov/pub/eph/planets/ioms/de405.iom.pdf> (accessed on 1 August 2021).
38. McCarthy, D.D.; Petit, G. IERS Conventions (2003). *IERS Tech. Note* **2004**, *32*, 1.
39. Vielberg, K.; Kusche, J. Extended forward and inverse modeling of radiation pressure accelerations for LEO satellites. *J. Geod.* **2020**, *94*, 43. [[CrossRef](#)]
40. Bruinsma, S. The DTM-2013 thermosphere model. *J. Space Weather Space Clim.* **2015**, *5*, A1. [[CrossRef](#)]
41. ILRS. SLRF2014 Station Coordinates. 2020. Available online: [ftp://gdc.cddis.eosdis.nasa.gov/pub/slr/products/resource/SLRF2014\\_POS+VEL\\_2030.0\\_200325.snx](ftp://gdc.cddis.eosdis.nasa.gov/pub/slr/products/resource/SLRF2014_POS+VEL_2030.0_200325.snx) (accessed on 1 August 2021).
42. Mendes, V.B.; Pavlis, E.C. High-accuracy zenith delay prediction at optical wavelengths. *Geophys. Res. Lett.* **2004**, *31*. [[CrossRef](#)]
43. Hugentobler, U.; Montenbruck, O. Satellite Orbits and Attitude. In *Springer Handbook of Global Navigation Satellite Systems*; Teunissen, P.J.G., Montenbruck, O., Eds.; Springer International Publishing: Cham, Switzerland, 2017; pp. 59–90.
44. Dewitte, S.; Clerbaux, N. Measurement of the Earth Radiation Budget at the Top of the Atmosphere—A Review. *Remote Sens.* **2017**, *9*, 1143. [[CrossRef](#)]
45. Montenbruck, O.; Gill, E.; Lutze, F.H. Satellite Orbits: Models, Methods, and Applications. *Appl. Mech. Rev.* **2002**, *55*, B27. [[CrossRef](#)]
46. Pearlman, M.R.; Degnan, J.J.; Bosworth, J.M. The international laser ranging service. *Adv. Space Res.* **2002**, *30*, 135–143. [[CrossRef](#)]
47. Strugarek, D.; Sosnica, K.; Jäggi, A. Characteristics of GOCE orbits based on Satellite Laser Ranging. *Adv. Space Res.* **2019**, *63*, 417–431. [[CrossRef](#)]
48. Strugarek, D.; Sośnica, K.; Zajdel, R.; Bury, G. Detector-specific issues in Satellite Laser Ranging to Swarm-A/B/C satellites. *Measurement* **2021**, *182*, 109786. [[CrossRef](#)]
49. Luthcke, S.B.; Zelensky, N.P.; Rowlands, D.D.; Lemoine, F.G.; Williams, T.A. The 1-Centimeter Orbit: Jason-1 Precision Orbit Determination Using GPS, SLR, DORIS, and Altimeter Data Special Issue: Jason-1 Calibration/Validation. *Mar. Geod.* **2010**, *26*, 399–421. [[CrossRef](#)]
50. Haines, B.; Bar-Sever, Y.; Bertiger, W.; Desai, S.; Willis, P. One-Centimeter Orbit Determination for Jason-1: New GPS-Based Strategies. *Mar. Geod.* **2004**, *27*, 299–318. [[CrossRef](#)]
51. Zajdel, R.; Sosnica, K.; Bury, G. A New Online Service for the Validation of Multi-GNSS Orbits Using SLR. *Remote Sens.* **2017**, *9*, 1049. [[CrossRef](#)]
52. Pearlman, M.; Arnold, D.; Davis, M.; Barlier, F.; Biancale, R.; Vasiliev, V.; Ciufolini, I.; Paolozzi, A.; Pavlis, E.C.; Sośnica, K.; et al. Laser geodetic satellites: A high-accuracy scientific tool. *J. Geod.* **2019**, *93*, 2181–2194. [[CrossRef](#)]
53. Zhou, X.; Chen, H.; Fan, W.; Zhou, X.; Chen, Q.; Jiang, W. Assessment of single-difference and track-to-track ambiguity resolution in LEO precise orbit determination. *GPS Solut.* **2021**, *25*, 62. [[CrossRef](#)]